Supporting Information

Schmierer *et al.* 10.1073/pnas.0710134105

SI Text

Model Conception: Available Prior Information and Assumptions Concerning Network Topology. It is clear that the R-Smads Smad2 and Smad3 and Smad4 shuttle between nucleus and cytoplasm in the absence and the presence of a signal (1–4). R-Smads can only be phosphorylated in the cytoplasm, because the receptors are membrane-bound. In contrast, the phosphatase targeting R-Smads has been reported to be enriched in the nucleus (5). Thus, both R-Smad phosphorylation and dephosphorylation are treated as irreversible in their respective compartment.

Phosphorylated R-Smads form complexes with Smad4, but also homomeric complexes with themselves (6). There is good evidence for the formation of heterotrimeric Smad complexes on DNA (7) and *in vitro* (8). The exact complex stoichiometries *in vivo* are, however, subject to debate (9). There is no kinetic information available about how and in which order heterotrimeric complexes would form, and nothing is known about the behavior of putative dimeric intermediates. For these reasons, the model makes the simplifying assumption that Smad complexes are homodimers and heterodimers rather than trimers. Smad complex association and dissociation are assumed to take place in both the nucleus and cytoplasm, as there is no experimental evidence to suggest otherwise. Both reactions are considered reversible, and complexes thus continuously form and unform in both compartments.

Pronounced inhibition of nuclear export of Smad complexes has been shown to be a key event in nuclear Smad accumulation in response to TGF-β (10–12). Whether this is predominantly because Smad complexes are efficiently retained in the nucleus by interactions with nuclear molecules (12) or because the structural motifs required for Smad export are masked by complex formation (10) is irrelevant for the kinetic model. Here, we assume that Smad complexes have to dissociate before nuclear export of their subunits. The C-terminal serine phosphates of the R-Smads are an integral part of the surface of the Smad–Smad interaction and are thus buried within Smad complexes (8). Therefore, we consider it likely that the nuclear Smad phosphatase can act only on monomeric and not on complexed phospho-Smad2.

Monomeric phospho-Smad2 cannot be observed experimentally and is assumed to freely shuttle between nucleus and cytoplasm. This assumption is supported by the finding that the nuclear import and export rate constants measured for the mutant Smad2 D300H, which is phosphorylated in response to a signal but cannot form Smad complexes, are not significantly different in the absence and in the presence of TGF-β (data not shown).

Within the modeling period of 2.5 h and independent of the absence or presence of TGF-β, there is no detectable turnover of Smads as judged by stable Smad levels in the presence of the translation inhibitor cycloheximide (1, 2). Thus, irrespective of the absence or presence of a signal, the mean life time of Smads is much longer than the modeled time period. The same applies for the type I receptor ALK5 (data not shown), and we consider expression levels of all involved proteins constant within the period of interest.

Finally, we treat the two R-Smads that are phosphorylated in response to TGF-β as a single species and assume that Smad3 undergoes identical reactions to Smad2.

Kinetic Measurements and Kinetic Assumptions. To minimize the number of kinetic parameters, all reactions were approximated by mass action kinetics. The reaction sequence forming the receptor activation module (13) was described by a single, irreversible mass action reaction equation, where binding of TGF-β converts inactive receptors into active receptors. The import and export rate constants (k_{in} = 0.0026 s^{-1} and k_{ex} = 0.0056 s^{-1}) for the constitutive shuttling of Smad2 were measured by whole compartment FRAP of nuclear EGFP-Smad2 (12) (Fig. S1*A*). Briefly, nuclei of unstimulated cells were photobleached and the reappearance of fluorescence in the nucleus was monitored until a steady state was reached. The resulting recovery curves are monophasic and can be described by a single exponential, indicating that nuclear import and export are indeed governed by mass action kinetics. The solution of the corresponding rate equation was fitted to averaged data (n = 10) by parameter variation, and best-fit values for k_{in} and k_{ex} were obtained. The same value k_{in} was also used for Smad4 import, because we have good evidence that Smad4 import occurs with comparable rate to that of Smad2 (unpublished data). However, Smad4 is equally distributed between nucleus and cytoplasm before TGF-β stimulation (3), indicating that its import and export rate constants are very similar. The Smad4 export rate constant was thus set to the same value as its import rate constant.

Because the presence of immobile fractions of EGFP-Smad2 in either the nucleus and/or the cytoplasm would affect our measurements of import and export rate constants and potentially also the subsequent model fits, we have also performed intracompartmental FRAP experiments to test for the presence of such immobile fractions. However, >95% recovery was observed within <3 min, irrespective of the compartment studied and the absence or the presence of TGF-β (data not shown). Recovery was not significantly different from 100%, indicating that EGFP-Smad2 can be considered fully mobile in both compartments.

Independent of the compartment they reside in, identical affinities were assigned to all Smad complexes, whether heteromeric or homomeric. This simplifying assumption is supported by the similarity of the binding interfaces of Smad2 and Smad4 that are involved in complex formation (8, 9). To relate the nuclear import rate of Smad complexes to the nuclear import rate of monomeric Smads, we introduced a parameter termed complex import factor (CIF), which is equal to the fold difference between the import rate of Smad complexes and the import rate of monomeric Smads. In the RO model, CIF was fixed to 1, i.e., import of Smad complexes proceeds with the same rate as import of monomeric Smads. In the RECI model, the restriction of CIF = 1 was lifted and CIF was subjected to parameter optimization.

Model Calibration: Definition of the Initial Steady State Without TGF-β. For calibration purposes, we estimated a total number of 100,000 particles of Smad2 plus Smad3 per cell and 100,000 particles of Smad4 per cell by comparing known amounts of recombinant proteins with cell extracts on immunoblots (ref. 14 and data not shown). Absolute amounts of EGFP-Smad2 in the HaCaT EGFP-Smad2 cell line were quantified relative to the estimates for the endogenous R-Smads by immunoblotting (12) and immunofluorescence (Fig. S1*B*) performed as described (3) on parental HaCaT cells and HaCaT EGFP-Smad2 cells with anti-Smad2/3 antibodies (BD Biosciences). Cells were imaged with a ×10 objective, and average fluorescence intensities were determined with ImageJ 1.37v software. Both methods showed

that EGFP-Smad2 is expressed close to endogenous levels, thus corresponding to ≈100,000 EGFP-Smad2 molecules per cell.

Concentrations of the receptor kinase and the phosphatase can be set arbitrarily. Because we assume mass action kinetics and constant levels of receptor and phosphatase, doubling the amount of receptor would simply cause a corresponding decrease in the estimate for the phosphorylation constant by a factor of two. The same applies for the relationship between phosphatase concentration and, in this case, the dephosphorylation constant. For simplicity, we set both the concentration of the type I receptor kinase and the phosphatase to unity, i.e., 1 nM.

In the absence of TGF-β, the only reactions taking place are constitutive nucleocytoplasmic shuttling of Smad2 and Smad4, which are both at steady state. The cytoplasmic/nuclear distribution of Smad2 is defined by the ratio k_{ex} over k_{in}. The value measured kinetically was 2.1, which is in excellent agreement with the observed nucleocytoplasmic distribution of EGFP-Smad2 (12). As discussed above, Smad4 is equally distributed between the nucleus and cytoplasm. Together, these parameters give a full description of the steady state in HaCaT EGFP-Smad2 cells before a TGF-β signal and thus provide a complete set of initial conditions for the system (Table S1).

Fluorescence data are proportional to concentrations, whereas immunoblot data are proportional to total particle numbers. To use both types of data, particle numbers in nucleus and cytoplasm were converted into the corresponding concentrations. For this conversion, the nucleocytoplasmic volume ratio is an important parameter and was determined experimentally. Briefly, HaCaT EGFP-Smad2 cells were treated with TGF-β, and both nuclear and cytoplasmic fluorescence was monitored during the nuclear accumulation process. The fluorescence intensities measured are proportional to concentrations rather than particle numbers. Thus, a particle flux from the cytoplasm into the nucleus that reduces cytoplasmic fluorescence by $-\Delta F_{cyt}$ causes an increase in nuclear fluorescence of $\Delta F_{nuc} = A \cdot \Delta F_{cyt}$, where A is the ratio of accessible cytoplasmic to accessible nuclear volume. A is thus given by the ratio of nuclear fluorescence increase over cytoplasmic fluorescence decrease $A = \Delta F_{nuc} / \Delta F_{cyt}$. A value of 2.3 ± 0.3 ($n = 10$) was obtained, which is in good agreement with previous results (12). With this volume ratio and an estimated nuclear volume of 1 pl, the cytoplasmic volume was set to 2.3 pl.

Curve Fitting and Parameter Estimation. EGFP-Smad2 nuclear accumulation, EGFP-Smad2 nuclear clearance, and Smad2 phosphorylation data were fitted simultaneously. The observed nucleocytoplasmic distribution of phospho-Smad2 ($\leq 16\% \pm 2\%$ of phospho-Smad2 in the cytoplasm) was used as a constraint. With this constraint in place, the RO model failed to fit the data. Thus, for the RO model, this constraint had to be lifted. The optimal parameter set for either the RO model or the RECI model were found by using optimizers provided in COPASI (15). Several algorithms were tested, such as the Hooke and Jeeves algorithm, the genetic algorithm (GA), and a simulated annealing method. These methods reliably converged to the same unique minimum in parameter space, which we thus considered to be the global minimum. Optimization methods relying on the derivative of the fitting function, such as steepest descent and Levenberg-Marquardt, more frequently terminated within local minima. Our confidence in the global minimum found was increased by performing multiple optimizations from random starting values and arriving at the same global minimum. Importantly, each parameter in this optimal parameter set was found within a biologically meaningful range.

The Best-Fit Parameter Sets. By simultaneously fitting the datasets presented in Fig. 2, seven parameters were optimized in the RECI model and six parameters were optimized in the RO model. The optimal set of parameters found for each model (Fig. 2) was used for all subsequent simulations.

The following parameters were optimized:

Rate constant for receptor activation, $k_{TGF\text{-}\beta}$. Binding of TGF-β to the receptor is considered an irreversible reaction that leads to full activation of the receptor kinase.

Rate constant for R-Smad phosphorylation, k_{phos}. The rate constant k_{phos} is obtained for a fixed cytoplasmic receptor concentration of unity (1 nM).

Rate constant for R-Smad dephosphorylation, k_{dephos}. The rate constant k_{dephos} is obtained for a fixed nuclear phosphatase concentration of unity (1 nM).

Dissociation constant of Smad complexes, K_{diss}. Smad complex stability is characterized by the complex dissociation constant K_{diss}, which is the ratio of two kinetic parameters, k_{off} [s^{-1}] over k_{on} [$nM^{-1} \cdot s^{-1}$]. For Smad-Smad complexes, we estimated an off-rate k_{off} of 0.016 s^{-1}, corresponding to a mean complex life time of ≈1 min. The value of k_{off} does not influence system behavior significantly (see Fig. 5*D*). K_{diss} was then optimized and the corresponding on-rate was calculated from the optimized K_{diss} and the estimated off-rate.

Relative complex import rate CIF. CIF is the fold difference between import rate for Smad complexes and the import rate of monomeric Smad. CIF was set to unity in the RO model (complexes are imported with identical rates to monomeric Smads). In the RECI model, CIF was subjected to parameter optimization.

The dissociation constant of the receptor kinase/SB-431542 (SB) binding, K_{dissSB}. SB is an ATP-competitive inhibitor that, at a concentration of ≈400–800 nM, inhibits TGF-β-dependent gene transcription by 50% (16). These values were used as boundary values for the optimization of K_{dissSB}, the dissociation constant of the receptor/SB interaction. The off-rate of the receptor/SB-431542 interaction k_{offSB} was estimated at 100 s^{-1}, corresponding to a mean binding time of 0.01 s. The on-rate k_{onSB} can be calculated by dividing k_{offSB} by K_{dissSB}.

Total endogenous phospho-Smad2, $pS2_{tot}$. This scaling parameter converts relative band intensities from phospho-Smad2 immunoblots, into absolute particle numbers of total endogenous phospho-Smad2. $pS2_{tot}$ thus is the number of phosphorylated, endogenous Smad2 molecules per cell after 45 min of TGF-β treatment.

A Comparison of the Best-Fit Parameter Sets Reveals Why the RO Model Fails to Fit All Datasets. Although not immediately intuitive, the failure of the RO model to fit the phosphorylation data (Fig. 2*E*) together with the nuclear accumulation and nuclear clearance data (Fig. 2*D*) can be explained by comparing the parameter values obtained for each model. In the RO model, Smad complexes are imported into the nucleus more slowly than in the RECI model. Thus, to correctly describe the kinetics of nuclear Smad2 accumulation in response to TGF-β (Fig. 2*D*), the equally good RO model fit requires faster receptor activation and Smad phosphorylation than the RECI model (Fig. 2*G*; $k_{TGF\text{-}\beta}$ and k_{phos}). These requirements, however, force the RO model to overestimate the rate of build-up of total phospho-Smad2 (Fig. 2*G*; $pS2_{tot}$), and it fails to accurately fit the phosphorylation kinetics (Fig. 2*E*). Moreover, the slower complex import in the RO model compared with the RECI model causes a backlog of phospho-Smad2 in the cytoplasm, which is exacerbated further by faster Smad2 activation. This backlog then explains the far too high fraction of cytoplasmic phospho-Smad2 that the RO model predicts (Fig. 2*F*).

Statistical Analysis of the Best-Fit Parameter Set. Because of experimental errors and variations inherent in any biological system, some parameter values can be varied considerably around their best-fit value, and the fit obtained will still be within the error bars of all experiments. Thus, the optimal parameter set found

through rigorous minimization is in practice only the best-fitting or most probable example out of an ensemble of biologically relevant parameter sets that all produce a reasonable fit. To obtain confidence intervals for the parameters, we statistically explored the neighborhood of the best-fit parameter set. One-thousand runs of the GA search in COPASI were performed. Each GA run consisted of 100 generations with a population size of 20. Starting values for each run were picked at random from intervals spanning two to three orders of magnitude around the best-fit value. Where possible, intervals were restricted to span biologically meaningful ranges. For instance, the complex dissociation constant was constrained between 1 and 1,000 nM (17). Because 100 generations are not sufficient to arrive at the unique best-fit parameter set, this partial optimization procedure yielded parameter sets in the neighborhood of the best-fit parameter set. Of the 1,000 sets calculated, the 500 with the best goodness of fit values were considered potentially valid sets and subjected to a statistical analysis. The minimal value, the maximal value, mean, median, 5% quantile, and 95% quantile were calculated for each parameter. Moreover, parameters were plotted against each other to identify parameter correlations.

The statistics of the distributions of the parameter values found are shown in Fig. S4*A*. Most parameters are distributed within narrow ranges that are well within the limits that were imposed. However, in some cases, the minimal or maximal parameter value found is equal to the imposed upper or lower limit, respectively. This indicates that, mathematically, higher or lower values than the imposed limits are possible. This is the case for K_{dissSB}, CIF, and K_{diss}. K_{dissSB} can in principle be both <400 nM and >800 nM; however, these comparably narrow bounds are imposed by experimental evidence (16). In the case of CIF, the distribution is wide because CIF ceases to significantly influence the dynamics of the system when it is large. Thus, solutions with a CIF larger than the used boundary value of 100 are mathematically possible and we cannot give an upper limit for the value of CIF. More importantly, however, we can give a lower limit for CIF at 2.3, i.e., Smad complexes have to be imported more than twice as fast as monomeric Smads to fit all datasets. In the case of K_{diss}, the wide distribution is caused by a strong anticorrelation with k_{dephos} (see the next section).

Parameter Correlation Analysis. In a plot of k_{dephos} against K_{diss} values from the best 500 parameter sets obtained, the extreme anticorrelation between these two parameters becomes apparent (Fig. S4*B*). Two regimes can be identified, which correspond to the extremes of the correlation plot. In one extreme, dephosphorylation is fast compared with Smad complex dissociation, and dissociation becomes rate limiting for both reactions (dissociation regime). In the other extreme, complexes are relatively unstable and dephosphorylation becomes rate-limiting (dephosphorylation regime). In the dissociation regime, k_{dephos} can take on high values without significantly affecting the dynamics of the system. Correspondingly, in the dephosphorylation regime, the value of K_{diss} can take on high values without significantly perturbing the dynamics of the system. Because of this strong anticorrelation, these two constants cannot be disentangled, and fits of the experimental data only give an estimate for the individual values for K_{diss} and k_{dephos}. However, their product is a well constrained parameter. Notably, the majority of solutions are found at the transition between both regimes, corresponding to low values for both K_{diss} and K_{dephos}. This suggests that, in the cell, the system might operate in the mixed regime, with neither of the two parameters being clearly rate-limiting. Thus, both parameters are possible points of control, which also becomes apparent in the sensitivity analysis, where the system proves to be highly sensitive to both. All other parameters showed only weak correlation when plotted against each other (data not shown).

Sensitivity Analysis. In this type of analysis, individual parameters are varied and the effect of such variation on the output of the system is calculated. The steady-state concentration of nuclear Smad2/Smad4 complexes (i.e., the nuclear concentration of the transcriptionally active species) was defined as system output. The results are given in Fig. 5*D* as scaled sensitivity coefficients, ε, which are defined as:

$$\varepsilon_{k_i} = \frac{\partial [S24]_N}{\partial k_i} \cdot \frac{k_i}{[S24]_N},$$

where $[S24]_N$ is the plateau concentration of nuclear Smad2/4 complexes at steady state, and k_i is the individual parameters. A positive value of ε indicates an increase, and a negative value indicates a decrease in the system output upon increase of the respective parameter. The absolute value of ε is a measure for the magnitude of the effect and describes the sensitivity of the output to a change in the respective parameter.

1. Inman GJ, Nicolas FJ, Hill CS (2002) Nucleocytoplasmic shuttling of Smads 2, 3, and 4 permits sensing of TGF-β receptor activity. *Mol Cell* 10:283–294.
2. Nicolás FJ, De Bosscher K, Schmierer B, Hill CS (2004) Analysis of Smad nucleocytoplasmic shuttling in living cells. *J Cell Sci* 117:4113–4125.
3. Pierreux CE, Nicolás FJ, Hill CS (2000) TGF-β-independent shuttling of Smad4 between the cytoplasm and nucleus. *Mol Cell Biol* 20:9041–9054.
4. Xu L, Kang Y, Col S, Massagué, J (2002) Smad2 nucleocytoplasmic shuttling by nucleoporins CAN/Nup214 and Nup153 feeds TGF-β signaling complexes in the cytoplasm and nucleus. *Mol Cell* 10:271–282.
5. Lin X, *et al.* (2006) PPM1A functions as a Smad phosphatase to terminate TGF-β signaling. *Cell* 125:915–928.
6. Liu F, Pouponnot C, Massagué, J (1997) Dual role of the Smad4/DPC4 tumor suppressor in TGF-β-inducible transcriptional complexes. *Genes Dev* 11:3157–3167.
7. Inman GJ, Hill CS (2002) Stoichiometry of active Smad-transcription factor complexes on DNA. *J Biol Chem* 277:51008–51016.
8. Wu JW, *et al.* (2001) Crystal structure of a phosphorylated Smad2: Recognition of phosphoserine by the MH2 domain and insights on Smad function in TGF-β signaling. *Mol Cell* 8:1277–1289.
9. Wu JW, Fairman R, Penry J, Shi Y (2001) Formation of a stable heterodimer between Smad2 and Smad4. *J Biol Chem* 276:20688–20694.
10. Chen HB, Rud JG, Lin K, Xu L (2005) Nuclear targeting of transforming growth factor-β-activated Smad complexes. *J Biol Chem* 280:21329–21336.
11. Dudu V, *et al.* (2006) Postsynaptic mad signaling at the *Drosophila* neuromuscular junction. *Curr Biol* 16:625–635.
12. Schmierer B, Hill CS (2005) Kinetic analysis of Smad nucleocytoplasmic shuttling reveals a mechanism for TGF-β-dependent nuclear accumulation of Smads. *Mol Cell Biol* 25:9845–9858.
13. Vilar JM, Jansen R, Sander C (2006) Signal processing in the TGF-β superfamily ligand-receptor network. *PLoS Comput Biol* 2:e3.
14. Clarke DC, Betterton MD, Liu X (2006) Systems theory of Smad signaling. *Syst Biol* 153:412–424.
15. Hoops S, *et al.* (2006) COPASI: A complex pathway simulator. *Bioinformatics* 22:3067–3074.
16. Inman GJ, *et al.* (2002) SB-431542 is a potent and specific inhibitor of TGF-β superfamily type I activin receptor-like kinase (ALK) receptors ALK4, ALK5, and ALK7. *Mol Pharmacol* 62:65–74.
17. Aldridge BB, Burke JM, Lauffenburger DA, Sorger PK (2006) Physicochemical modeling of cell signaling pathways. *Nat Cell Biol* 8:1195–1203.

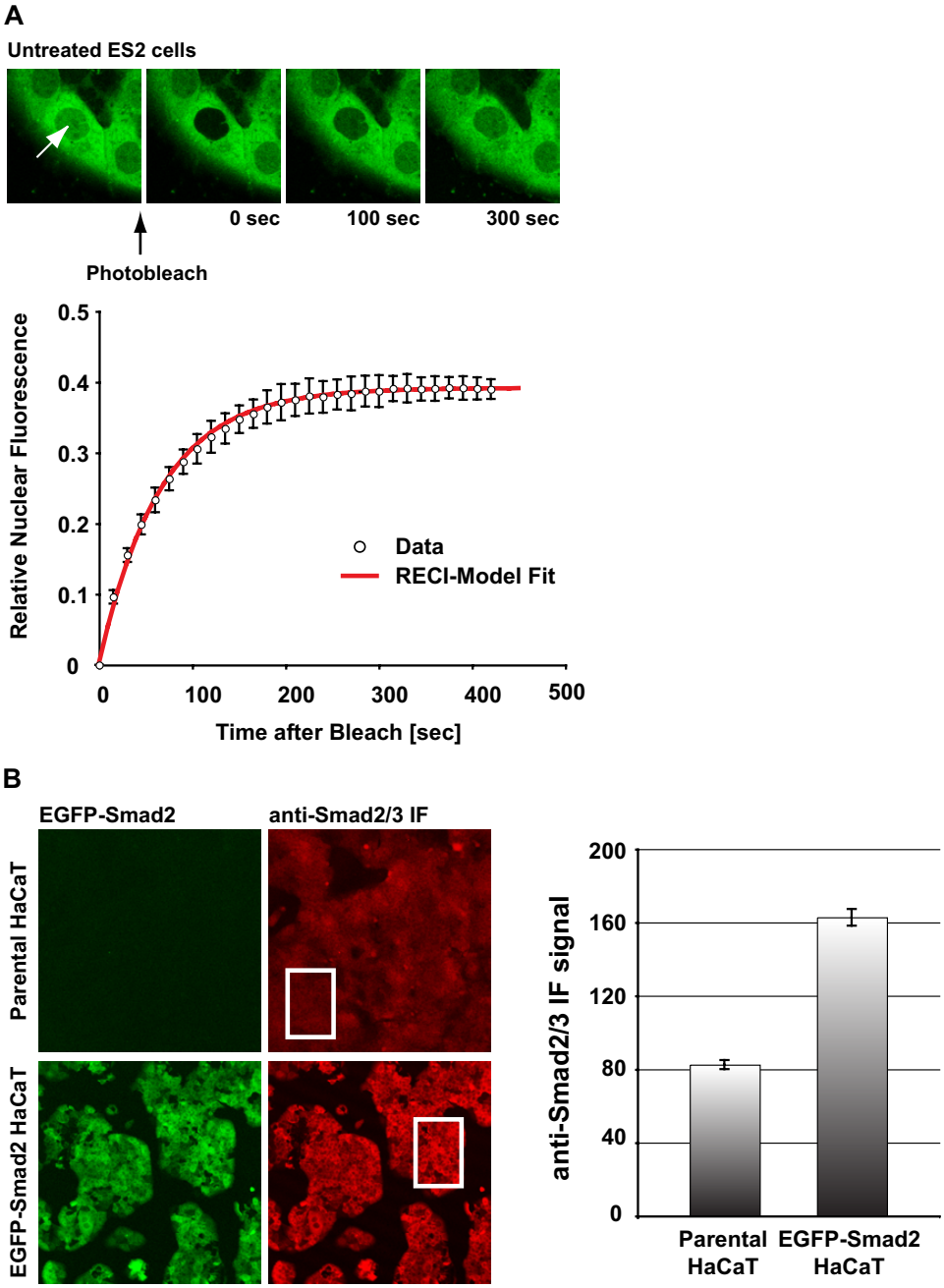

Fig. S1. Smad2 shuttling under basal conditions and quantification of EGFP-Smad2 expression. (*A*) Nuclear import and export rate constants for EGFP-Smad2. (*Upper*). In the absence of TGF-β, basal nucleocytoplasmic shuttling of Smad2 and Smad4 is the only reaction taking place, and both are at steady state. Photobleaching of the nuclear proportion of EGFP-Smad2 disturbs this steady state, and from the fluorescence recovery curve, k_{in} and k_{ex} were obtained by curve fitting as described (1). Images from a representative experiment are shown. (*Lower*) Experimental data points are indicated by open circles ($n = 10$, $\pm$ SD) and are plotted relative to the cytoplasmic fluorescence directly after the bleach. The solid line represents the RECI model fit calculated with the obtained values $k_{in} = 0.0026\ s^{-1}$ and $k_{ex} = 0.0056\ s^{-1}$. (*B*) EGFP-Smad2 is expressed at approximately endogenous levels. Expression levels of EGFP-Smad2 in the HaCaT EGFP-Smad2 cell line were estimated by comparing immunofluorescence (IF) signals in these cells with signals obtained in parental HaCaTs. Both cell lines were fixed and stained with anti-Smad2/3 antibodies. Pictures were taken on a confocal microscope with a $\times 10$ objective, and average fluorescence intensities were determined for identical areas. A representative picture is shown, and the white boxes indicate a representative measurement area. The result confirmed a previous estimate obtained by immunoblotting (1), indicating that levels of EGFP-Smad2 are approximately equal to the combined levels of endogenous Smad2 and Smad3.

1. Schmierer B, Hill CS (2005) Kinetic analysis of Smad nucleocytoplasmic shuttling reveals a mechanism for TGF-β-dependent nuclear accumulation of Smads. *Mol Cell Biol* 25:9845–9858.

A Reaction Network

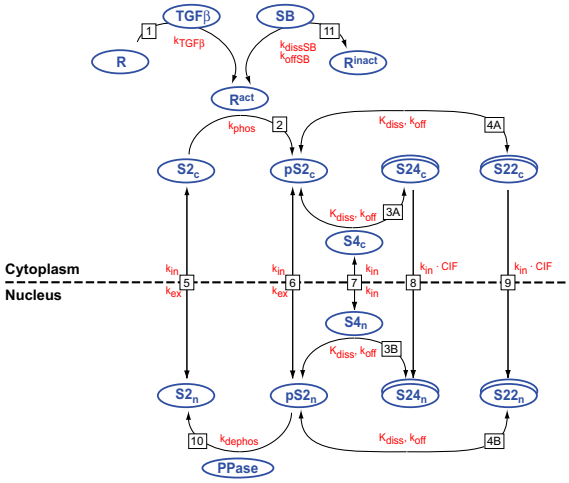

B Chemical Equations

Basic reactions

1	$R + TGF\beta \xrightarrow{k_{TGF\beta}} R^{act}$	Receptor Activation
2	$R^{act} + S2_c \xrightarrow{k_{phos}} R^{act} + pS2_c$	Phosphorylation
3A, 3B, 4A, 4B	$pS2_c + S4_c \rightleftharpoons S24_c$; $pS2_n + S4_n \rightleftharpoons S24_n$; $2\,pS2_c \rightleftharpoons S22_c$; $2\,pS2_n \rightleftharpoons S22_n$; $K_{diss} = k_{off}/k_{on}$	Complex Formation
5, 6, 7	$S2_c \rightleftharpoons S2_n$; $pS2_c \rightleftharpoons pS2_n$; $S4_c \rightleftharpoons S4_n$	Nucleocytoplasmic Shuttling
8, 9	$S24_c \xrightarrow{k_{in} \cdot CIF} S24_n$; $S22_c \xrightarrow{k_{in} \cdot CIF} S22_n$	Complex Import
10	$pS2_n + PPase \xrightarrow{k_{dephos}} S2_n + PPase$	Dephosphorylation
11	$R^{act} + SB \rightleftharpoons R^{inact}$	Receptor Inhibition

C Ordinary Differential Equations

$$\frac{d[R]}{dt} = -k_{TGF\beta}[R][TGF\beta]$$

$$\frac{d[TGF\beta]}{dt} = -k_{TGF\beta}[R][TGF\beta]$$

$$\frac{d[R^{act}]}{dt} = k_{TGF\beta}[R][TGF\beta] - k_{onSB}[R^{act}][SB] + k_{offSB}[R^{inact}]$$

$$\frac{d[R^{inact}]}{dt} = k_{onSB}[R^{act}][SB] - k_{offSB}[R^{inact}]$$

$$\frac{d[SB]}{dt} = k_{offSB}[R^{inact}] - k_{onSB}[R^{act}][SB]$$

$$\frac{d[S2]_c}{dt} = k_{ex}[S2]_n - k_{in}[S2]_c - k_{phos}[S2]_c[R^{act}]$$

$$\frac{d[pS2]_c}{dt} = k_{ex}[pS2]_n - k_{in}[pS2]_c + k_{phos}[S2]_c[R^{act}] - k_{on}[pS2]_c([S4]_c + 2[pS2]_c) + k_{off}([S24]_c + 2[S22]_c)$$

$$\frac{d[S4]_c}{dt} = k_{in}[S4]_n - k_{in}[S4]_c - k_{on}[S4]_c[pS2]_c + k_{off}[S24]_c$$

$$\frac{d[S24]_c}{dt} = k_{on}[pS2]_c[S4]_c - k_{off}[S24]_c - k_{in}CIF[S24]_c$$

$$\frac{d[S22]_c}{dt} = k_{on}[pS2]_c^2 - k_{off}[S22]_c - k_{in}CIF[S22]_c$$

$$\frac{d[S2]_n}{dt} = k_{in}[S2]_c - k_{ex}[S2]_n + k_{dephos}[pS2]_n[PPase]$$

$$\frac{d[pS2]_n}{dt} = k_{in}[pS2]_c - k_{ex}[pS2]_n - k_{dephos}[pS2]_n[PPase] - k_{on}[pS2]_n([S4]_n + 2[pS2]_n) + k_{off}([S24]_n + 2[S22]_n)$$

$$\frac{d[S4]_n}{dt} = k_{in}[S4]_c - k_{in}[S4]_n - k_{on}[S4]_n[pS2]_n + k_{off}[S24]_n$$

$$\frac{d[S24]_n}{dt} = k_{on}[pS2]_n[S4]_n - k_{off}[S24]_n + k_{in}CIF[S24]_c$$

$$\frac{d[S22]_n}{dt} = k_{on}[pS2]_n^2 - k_{off}[S22]_n + k_{in}CIF[S22]_c$$

Abbreviations used:

R	unbound receptor
R^{act}	TGF-β-activated receptor
R^{inact}	SB-431542 bound receptor
SB	SB-431542
S2	Smad2
pS2	phospho-Smad2
S4	Smad4
S24	Smad2/Smad4 complexes
S22	Smad2/Smad2 complexes
PPase	Phosphatase
c, n	cytoplasmic and nuclear, respectively

Fig. S2. From the reaction network to chemical equations and ODEs: Basic system for wild-type cells lacking EGFPSmad2. (*A*) The reaction network (see also Fig. 1*B*). The kinetic constants for the reactions are given in red. (*B*) Chemical reaction equations. Numbers link the chemical reactions to the reaction network shown in *A*. (*C*) The corresponding system of ODEs. [ ] indicates concentrations.

A Chemical Equations

Basic reactions

1	$R + TGF\beta \xrightarrow{k_{TGF\beta}} R^{act}$	Receptor Activation
2	$R^{act} + S2_c \xrightarrow{k_{phos}} R^{act} + pS2_c$	Phosphorylation
3A 3B 4A 4B	$pS2_c + S4_c \rightleftharpoons S24_c$ $pS2_n + S4_n \rightleftharpoons S24_n$ $2\,pS2_c \rightleftharpoons S22_c$ $2\,pS2_n \rightleftharpoons S22_n$ $K_{diss} = \frac{k_{off}}{k_{on}}$	Complex Formation
5 6 7	$S2_c \rightleftharpoons S2_n$ $pS2_c \rightleftharpoons pS2_n$ $S4_c \rightleftharpoons S4_n$	Nucleocytoplasmic Shuttling
8 9	$S24_c \xrightarrow{k_{in} \cdot CIF} S24_n$ $S22_c \xrightarrow{k_{in} \cdot CIF} S22_n$	Complex Import
10	$pS2_n + PPase \xrightarrow{k_{dephos}} S2_n + PPase$	Dephosphorylation
11	$R^{act} + SB \rightleftharpoons R^{inact}$	Receptor Inhibition

Additional chemical reactions involving EGFP-Smad2

	$R^{act} + G_c \xrightarrow{k_{phos}} R^{act} + pG_c$	Phosphorylation
	$pG_c + S4_c \rightleftharpoons G4_c$ $pG_n + S4_n \rightleftharpoons G4_n$ $2\,pG_c \rightleftharpoons GG_c$ $2\,pG_n \rightleftharpoons GG_n$ $pS2_c + pG_c \rightleftharpoons G2_c$ $pS2_n + pG_n \rightleftharpoons G2_n$ $K_{diss} = \frac{k_{off}}{k_{on}}$	Complex Formation
	$G_c \rightleftharpoons G_n$ $pG_c \rightleftharpoons pG_n$	Nucleocytoplasmic Shuttling
	$G4_c \xrightarrow{k_{in} \cdot CIF} G4_n$ $GG_c \xrightarrow{k_{in} \cdot CIF} GG_n$ $G2_c \xrightarrow{k_{in} \cdot CIF} G2_n$	Complex Import
	$pG_n + PPase \xrightarrow{k_{dephos}} G_n + PPase$	Dephosphorylation

R	unbound receptor
R^{act}	TGF-β-activated receptor
R^{inact}	SB-431542 bound receptor
SB	SB-431542
S2	Smad2
pS2	phospho-Smad2
S4	Smad4
S24	Smad2/Smad4 complexes
S22	Smad2/Smad2 complexes
PPase	Phosphatase
G	EGFP-Smad2
pG	Phosphorylated EGFP-Smad2
G4	EGFP-Smad2/Smad4 complexes
G2	EGFP-Smad2/Smad2 complexes
GG	EGFP-Smad2/EGFP-Smad2 complexes
c, n	cytoplasmic and nuclear, respectively

B Ordinary Differential Equations

$$\frac{d[R]}{dt} = -k_{TGF\beta}[R][TGF\beta]$$

$$\frac{d[TGF\beta]}{dt} = -k_{TGF\beta}[R][TGF\beta]$$

$$\frac{d[R^{act}]}{dt} = k_{TGF\beta}[R][TGF\beta] - k_{onSB}[R^{act}][SB] + k_{offSB}[R^{inact}]$$

$$\frac{d[R^{inact}]}{dt} = k_{onSB}[R^{act}][SB] - k_{offSB}[R^{inact}]$$

$$\frac{d[SB]}{dt} = k_{offSB}[R^{inact}] - k_{onSB}[R^{act}][SB]$$

$$\frac{d[S2]_c}{dt} = k_{ex}[S2]_n - k_{in}[S2]_c - k_{phos}[S2]_c[R^{act}]$$

$$\frac{d[G]_c}{dt} = k_{ex}[G]_n - k_{in}[G]_c - k_{phos}[G]_c[R^{act}]$$

$$\frac{d[pS2]_c}{dt} = k_{ex}[pS2]_n - k_{in}[pS2]_c + k_{phos}[S2]_c[R^{act}] - k_{on}[pS2]_c([S4]_c + 2[pS2]_c + [pG]_c) + k_{off}([S24]_c + 2[S22]_c + [G2]_c)$$

$$\frac{d[pG]_c}{dt} = k_{ex}[pG]_n - k_{in}[pG]_c + k_{phos}[G]_c[R^{act}] - k_{on}[pG]_c([S4]_c + [pS2]_c + 2[pG]_c) + k_{off}([G4]_c + [G2]_c + 2[GG]_c)$$

$$\frac{d[S4]_c}{dt} = k_{in}[S4]_n - k_{in}[S4]_c - k_{on}[S4]_c([pS2]_c + [pG]_c) + k_{off}([S24]_c + [G4]_c)$$

$$\frac{d[S24]_c}{dt} = k_{on}[pS2]_c[S4]_c - k_{off}[S24]_c - k_{in}CIF[S24]_c$$

$$\frac{d[G4]_c}{dt} = k_{on}[pG]_c[S4]_c - k_{off}[G4]_c - k_{in}CIF[G4]_c$$

$$\frac{d[S22]_c}{dt} = k_{on}[pS2]_c^2 - k_{off}[S22]_c - k_{in}CIF[S22]_c$$

$$\frac{d[G2]_c}{dt} = k_{on}[pG]_c[pS2]_c - k_{off}[G2]_c - k_{in}CIF[G2]_c$$

$$\frac{d[GG]_c}{dt} = k_{on}[pG]_c^2 - k_{off}[GG]_c - k_{in}CIF[GG]_c$$

$$\frac{d[S2]_n}{dt} = k_{in}[S2]_c - k_{ex}[S2]_n + k_{dephos}[pS2]_n[PPase]$$

$$\frac{d[G]_n}{dt} = k_{in}[G]_c - k_{ex}[G]_n + k_{dephos}[pG]_n[PPase]$$

$$\frac{d[pS2]_n}{dt} = k_{in}[pS2]_c - k_{ex}[pS2]_n - k_{dephos}[pS2]_n[PPase] - k_{on}[pS2]_n([S4]_n + 2[pS2]_n + [pG]_n) + k_{off}([S24]_n + 2[S22]_n + [G2]_n)$$

$$\frac{d[pG]_n}{dt} = k_{in}[pG]_c - k_{ex}[pG]_n - k_{dephos}[pG]_n[PPase] - k_{on}[pG]_n([S4]_n + [pS2]_n + 2[pG]_n) + k_{off}([G4]_n + [G2]_n + 2[GG]_n)$$

$$\frac{d[S4]_n}{dt} = k_{in}[S4]_c - k_{in}[S4]_n - k_{on}[S4]_n([pS2]_n + [pG]_n) + k_{off}([S24]_n + [G4]_n)$$

$$\frac{d[S24]_n}{dt} = k_{on}[pS2]_n[S4]_n - k_{off}[S24]_n + k_{in}CIF[S24]_c$$

$$\frac{d[G4]_n}{dt} = k_{on}[pG]_n[S4]_n - k_{off}[G4]_n + k_{in}CIF[G4]_c$$

$$\frac{d[S22]_n}{dt} = k_{on}[pS2]_n^2 - k_{off}[S22]_n + k_{in}CIF[S22]_c$$

$$\frac{d[G2]_n}{dt} = k_{on}[pG]_n[pS2]_n - k_{off}[G2]_n + k_{in}CIF[G2]_c$$

$$\frac{d[GG]_n}{dt} = k_{on}[pG]_n^2 - k_{off}[GG]_n + k_{in}CIF[GG]_c$$

Fig. S3. Chemical reactions and ODEs: Full system for cells expressing EGFP-Smad2. (*A*) Chemical reactions. The basic system (*Upper*; as in Fig. S2*B*) and the additional reactions introduced because of the presence of EGFP-Smad2 (*Lower*) are shown. (*B*) The corresponding system of ODEs for the full system in the presence of EGFP-Smad2. [ ] indicates concentrations. This equation system was used throughout.

A

Parameter statistics	Best	Min	Max	Mean	Median	quantiles 5%	quantiles 95%	Units
$k_{TGF\beta}$	0.074	0.049	0.146	0.073	0.070	0.056	0.102	$nM^{-1}s^{-1}$
k_{phos}	0.00040	0.00032	0.00041	0.00036	0.00036	0.00033	0.00040	$nM^{-1}s^{-1}$
CIF	5.7	2.3	100*	18.8	9.4	3.0	71.7	-
K_{diss}	8.7	1*	34.3	8.1	5.9	1.3	23.0	nM
$pS2_{tot}$	31138	22516	41088	28668	28468	24689	33754	Number
k_{dephos}	0.0066	0.0031	0.0297	0.0103	0.0077	0.0037	0.0242	$nM^{-1}s^{-1}$
K_{dissSB}	684	400*	800*	601	613	404	799	nM
$K_{diss} \cdot k_{dephos}$	0.057	0.028	0.11	0.049	0.044	0.030	0.086	s^{-1}

B

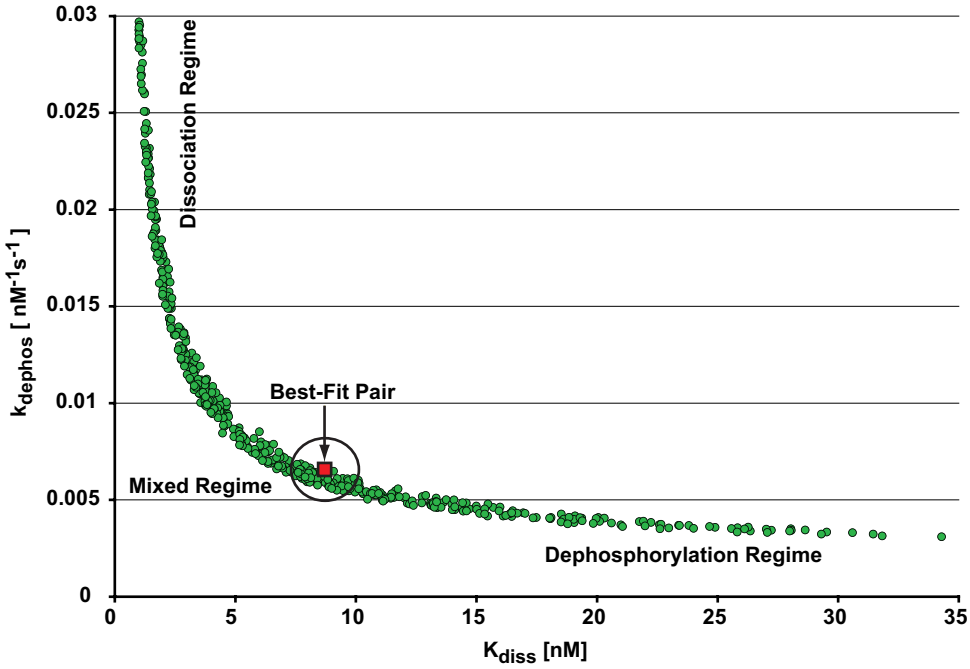

Fig. S4. Statistical analysis of the best-fit parameter set and parameter correlation. (*A*) Statistical analysis of the best-fit parameter set for the RECI model. To statistically explore the neighborhood of the best-fit parameter set, 1,000 runs of the parameter optimization procedure were performed from starting values randomly picked around the best-fit values. The 500 parameter sets with the best goodness of fit were considered potentially valid parameter sets. For each parameter, the best-fit value, the minimal value (Min) and the maximal value (Max), the mean, the median, 5% quantile, and 95% quantile are shown. In addition, the statistics for the product of K_{diss} and k_{dephos} are shown. Note that most parameters are constrained within narrow ranges, with the notable exceptions of CIF, the reason for which is discussed in the text, and the anticorrelated parameter pair K_{diss} and k_{dephos} (see *B*). The minimal and/or maximal value for some parameters was equal to the imposed limit, which is indicated by * and discussed in the text. (*B*) Strong anticorrelation was found for the dephosphorylation rate and the dissociation constant of Smad complexes. K_{diss} and k_{dephos} parameter pairs were obtained from the 500 best of 1,000 parameter sets and plotted. The pair from the best-fit set is indicated, as are the two distinct regimes defined by the relative values of K_{diss} and k_{dephos}. The overlap region indicates a mixed regime, where neither K_{diss} nor k_{dephos} are rate-limiting. Because of the strong anticorrelation, K_{diss} and k_{dephos} are less well constrained than other parameters and the uncertainty with regard to their values is larger. The product $K_{diss} \cdot k_{dephos}$, however, is a well constrained parameter (see *A*).

Table S1. Steady state in the absence of a signal

Reactants	Compartment	Particle numbers	Concentration, nM
Smad2/3 + EGFP-Smad2	Cytoplasm	82,800 + 82,800	60.6 + 60.6 = 121.2
Smad2/3 + EGFP-Smad2	Nucleus	17,200 + 17,200	28.5 + 28.5 = 57
Smad4	Cytoplasm	69,400	50.8
Smad4	Nucleus	30,600	50.8
All other Smad species	Any	0	0
Inactive receptors	Cytoplasm	1,400	1
Phosphatase	Nucleus	600	1
TGF-β	Cytoplasm*	0	0

*For the purposes of the modeling, binding of the ligand to the receptor is considered to occur in the cytoplasm.
The numbers given provide a full set of initial conditions before the addition of TGF-β. Particle numbers were rounded to the nearest hundred.